Tunable FSRS Measurements with Reduced Background Signals: Using an Etalon Filter to Generate Picosecond Pump Pulses in the 460-650 nm Range

Emmaline R. Lorenzo, Birendra Karki, Katie E. White, Kristen H. Burns,[1] Christopher G. Elles*

Department of Chemistry, University of Kansas, Lawrence, KS 66045 USA

*email: elles@ku.edu

Abstract

Generating wavelength-tunable picosecond laser pulses from an ultrafast laser source is essential for femtosecond stimulated Raman scattering (FSRS) measurements. Etalon filters produce narrowband (picosecond) pulses with an asymmetric temporal profile that is ideal for stimulated resonance Raman excitation. However, direct spectral filtering of femtosecond laser pulses is typically limited to the laser fundamental and harmonic frequencies due to very low transmission of broad bandwidth pulses through an etalon. Here, we show that a single etalon filter (15 cm^{-1} bandwidth, 172 cm^{-1} free spectral range) provides an efficient and tunable option for generating Raman pump pulses over a wide range of wavelengths when used in combination with an optical parametric amplifier and a second harmonic generation (SHG) crystal that has an appropriate phase-matching bandwidth for partial spectral compression before the etalon. Tuning the SHG wavelength to match individual transmission lines of the etalon filter gives asymmetric picosecond pump pulses over a range of 460-650 nm. Importantly, the SHG crystal length determines the temporal rise time of the filtered pulse, which is an important property for reducing background and increasing Raman signals compared with symmetric pulses having the same total energy. We examine the wavelength-dependent trade-off between spectral narrowing via SHG and the asymmetric pulse shape after transmission through the etalon. This approach provides a relatively simple and efficient method to generate tunable pump pulses with the optimum temporal profile for resonance-enhanced FSRS measurements across the visible region of the spectrum.

[1] Present Address: Department of Chemistry, Western Michigan University, Kalamazoo, MI 49008 USA

I. Introduction

Stimulated Raman scattering (SRS) and femtosecond stimulated Raman scattering (FSRS) are powerful vibrational spectroscopy techniques for studying the dynamics of chemical systems.[1-11] These nonlinear measurements take advantage of the frequency resolution from a narrowband picosecond (ps) pump pulse combined with the temporal resolution of a broadband femtosecond (fs) probe pulse to record the dephasing of optically induced vibrational coherences in the frequency domain.[12, 13] The temporal resolution is a result of the vibrational coherence being initiated only within the temporal envelope of the broadband (fs) probe pulse, whereas the spectral resolution depends on the bandwidth of the narrowband (ps) pump pulse.[14-17] An essential requirement of this mixed time-frequency domain measurement is the generation of narrowband pump pulses from an ultrafast laser source. The ability to tune the Raman excitation wavelength is also necessary in order to allow resonance enhancement of specific analytes, including transient species that would otherwise give Raman signals that are too weak to observe.[18-21]

Narrowband pump pulses are often generated using nonlinear optical techniques designed to give spectrally narrow output, or by direct spectral filtering of femtosecond laser pulses. Nonlinear techniques generally are more efficient and allow greater tunability. For example, narrowband optical parametric amplifiers (OPAs) produce Gaussian-shaped ps pulses directly,[22-24] whereas spectral compression via second harmonic generation (SC-SHG) using a long (few cm) pathlength SHG crystal provides an efficient way to convert the output from a traditional fs OPA into spectrally narrow ps pulses.[25-28] The SC-SHG approach generates pulses with a distorted temporal profile and typically requires additional spectral

filtering using a four focal plane (4*f*) filter.[25] Importantly, both of these nonlinear approaches ultimately produce ps pulses with symmetric temporal profiles that provide good frequency resolution, but also result in background contributions due to unwanted interactions between the leading edge of the pulse and the sample.[29] Such interactions deplete the population of target molecules and induce undesirable transient signals, including contributions from excited-state absorption (ESA), ground-state bleach (GSB), and stimulated emission (SE), all of which complicate the processing and interpretation of the stimulated Raman spectrum. Background signals are especially difficult to disentangle in the case of excited-state FSRS measurements, and represent one of the primary limitations of the technique.[30-32]

An alternative method of generating narrowband ps pump pulses with more favorable asymmetric temporal profiles uses a Fabry-Pérot etalon filter.[33, 34] Etalon filters rely on the interference between two highly reflective surfaces to transmit light only at wavelengths that match integer multiples of the pathlength between them.[35] Constructive interference at resonant wavelengths is responsible for "trapping" light within the mirror cavity, with the leakage of light in the forward direction resulting in transmission at discrete wavelengths. The reflectivity of the two mirrors and the distance between them determine the bandwidth of the transmission lines and the spacing between those lines, respectively. In the time domain, pulsed irradiation results in the transmission of light with an asymmetric temporal profile that represents the exponential decay of intensity as light escapes the etalon cavity. In other words, incident pulses with a relatively short duration are converted into asymmetric pulses with a profile that matches the rising edge of the incoming pulse, but has an

exponentially decaying tail from the ring-down of the cavity. If the pulse duration is short compared with the round-trip time of the etalon cavity, which occurs when the bandwidth of the incident pulse is larger than the spacing between the transmission lines, the temporal profile of the outgoing pulse will also be modulated at the difference frequency of the bands. Such oscillations can be eliminated through additional filtering to remove the side-bands in the frequency domain, or by using an etalon with a larger spacing between transmission lines.

In the context of SRS or FSRS measurements, the asymmetric pulse shape from an etalon filter helps to mitigate electronically resonant background signals by significantly reducing the number of pump photons that arrive before the broadband probe pulse initiates the vibrational coherence. Etalon filters have been used successfully in FSRS,[33, 36, 37] 2D-FSRS,[38-40] high resolution Raman imaging,[41, 42] and surface enhanced Raman spectroscopy (SERS) measurements.[43] However, the typical implementation uses etalon filters with relatively high finesse (≥100) in order to provide high spectral resolution and to avoid transmission in the side-bands. The finesse is defined as the ratio of the free spectral range (FSR; the spacing between transmission lines) and the bandwidth of the individual transmission lines.[35] The trade-off in using a high finesse etalon filter with a typical bandwidth of a few cm^{-1} is very low transmission efficiency for femtosecond laser pulses having a few hundred cm^{-1} of bandwidth, because most of the pulse energy is rejected by the filter. Thus, low throughput has traditionally limited this approach to the laser fundamental and harmonic frequencies, where low efficiency can be compensated by high incident power.

In this contribution, we demonstrate that a low-finesse etalon filter provides a valuable middle ground between the tunability of nonlinear optical techniques and the favorable temporal profile from direct spectral filtering with an etalon in order to generate optimally shaped ps laser pulses for broadband stimulated Raman measurements. The benefits of the asymmetric pulse profile are most pronounced for resonance Raman scattering, where background effects due to optical excitation can be significantly reduced compared with symmetric pulses. First, we demonstrate the broad wavelength tunability of the low finesse etalon filter over ~200 nm in the visible region (460-650 nm) and show how different conditions for second harmonic generation (SHG) preceding the etalon affect the resulting output pulse shape. A key point is that too much spectral narrowing in the SHG stage will eliminate the benefits of the etalon filter. Next, we examine the relationship between the rising edge of the asymmetric pump pulse and the magnitude of electronically resonant background signals in the resonance-enhanced SRS spectrum of the fluorescent dye rhodamine 6G (Rh6G). Finally, we highlight the superior performance of optimally shaped ps pulses for tunable resonance-enhanced SRS measurements by varying the excitation wavelength across the lowest-energy absorption band of Rh6G.

II. Experimental

We obtain Raman pump and probe pulses from the output of an amplified Ti:sapphire laser (Coherent, Legend Elite HP, 1kHz, 35 fs). We generate tunable pump pulses by directing a portion of the laser fundamental into an optical parametric amplifier (OPA), followed by one or two stages of second harmonic generation (SHG) using type-I BBO crystals. The final

stage of SHG uses a long pathlength crystal to limit the phase-matching bandwidth and produce spectrally narrow pump pulses, as described previously.[26] The length of the SHG crystal determines the initial bandwidth of the pump pulse (prior to spectral filtering), therefore we use crystals with path lengths of 2 mm (23.4°), 7 mm (22.8°), or 25 mm (21.1°), as indicated for each measurement. Figure S1 compares the representative spectral profiles for SHG at 555 nm using each of these three crystals.

The output from the BBO crystal passes through a custom air-spaced etalon filter (Light Machinery) with 25 μm separation and 85-90% reflectivity in the range 400-750 nm. Based on the transmission spectrum, the etalon filter has a FSR of 172 cm^{-1} and 15 cm^{-1} bandwidth, giving a finesse of ~11.5. The etalon is mounted on a manual rotation stage for fine-tuning the transmission frequency to match the output of the SHG crystal. After the etalon, the beam passes through a 4*f* spatial filter consisting of a dispersive grating (500 nm blaze wavelength, 1800 grooves/mm), a cylindrical lens (*f* = 200 mm), and an adjustable slit for limiting the bandwidth of the transmitted pulse. A planar mirror immediately behind the slit directs the beam back through the cylindrical lens and grating with a slight vertical offset in order to re-collimate the beam before it is attenuated and focused into a 2 mm cuvette containing the sample with a typical energy of 0.25-1.0 μJ/pulse. The overall efficiency depends on many factors (see below), but we typically attenuate the output of the OPA to achieve the desired pulse energy at the sample while also limiting the incident power at the etalon. In most cases, we use the 4*f* filter with a relatively wide slit width of 150 μm to remove satellite bands following transmission through the etalon (see Figure S2), however we also examine the slit width dependence over the range 30-150 μm. For comparison, we remove

the etalon for some measurements and use only the 4*f* spatial filter with a slit spacing of 30 μm to generate temporally symmetric Gaussian pump pulses with ~15 cm^{-1} bandwidth.

Changing the experimental conditions by tuning the Raman excitation wavelength, using a different BBO crystal length, or adding/removing the etalon filter is relatively straightforward. We tune the pump wavelength by changing the angle of the SHG crystal to match the output of the OPA. Changing the SHG crystal or adding/removing the etalon requires only minor realignment of the beam and a moderate change in pump-probe time delay of up to ~40 ps to compensate for the different arrival time at the sample. We maximize the overall throughput of the etalon filter by tuning the incident angle to match the peak intensity from SHG. The angle of the etalon and the placement of the slit in the 4*f* filter are optimized by observing the spectral profile of scattered Raman pump light in real time on the detector.

We obtain broadband (fs) probe pulses by focusing a second portion of the laser fundamental into a circularly translating CaF_2 disk for white-light continuum generation. A pair of parabolic mirrors collimate and then focus the probe beam into the sample, where it overlaps the pump beam with parallel (vertical) polarization. After the sample, the probe beam passes into a 1/4 m imaging spectrograph (Newport, MS260i) where a grating (1800 line/mm) disperses the light onto a 2068-pixel linear CCD array (Hamamatsu, S11155−2048-02). Using a 50 μm entry slit on the spectrograph provides an instrument-limited spectral resolution of ~10 cm^{-1}. The probe light is measured on the CCD at the full 1 kHz repetition rate and the Raman pump beam is blocked at 500 Hz for background subtraction. Each SRS spectrum that we report is an average over 4.5 x 10^5 laser shots for a baseline noise level <0.05 mOD, which is well below the limit required for the Raman spectra reported here.

Solvent Raman bands were used to calibrate the Raman frequency shift for each SRS spectrum prior to baseline correction (see Figure S3).

We measure the temporal profile of the Raman pump pulses by recording the time-dependent SRS signal of neat cyclohexane or methanol as a function of the delay between pump and probe pulses, and then integrating over the center bandwidth for one of these Raman bands (typically the 801 cm^{-1} band of cyclohexane or the 1033 cm^{-1} band of methanol). This approach (see Figure S4) gives an accurate representation of the temporal profile of the pump pulse.[16, 30] Each time-dependent spectrum represents the average of 4 scans with 3000 shots per time point and a 0.1 ps step size. We record the spectral intensity profile of the pump pulses by observing scattered light on the CCD array and averaging 8000 shots.

III. Results and Discussion

A. Picosecond Pulse Generation

We illustrate the broad wavelength tunability of the etalon filter by generating asymmetric ps pump pulses for SRS measurements at three different wavelengths. Figure 1a shows the transmission spectrum of the etalon across the entire visible region. Each one of the transmission lines, which have equal spacing of 172 cm^{-1}, is suitable for generating Raman pump pulses after tuning the OPA and SHG output into resonance. Importantly, the transmission efficiency of the etalon is limited by the 15 cm^{-1} bandwidth of the transmission line, and therefore requires prior spectral compression in order to allow sufficient throughput at the desired Raman pump wavelength. The degree of spectral compression

depends on the SHG crystal length (Figure S1), which is inversely proportional to the phase-matching bandwidth.[26] Figure 1 shows temporal profiles for the Raman pump pulses at representative wavelengths of 460, 545, and 650 nm, as well as the resulting SRS spectra for neat cyclohexane.

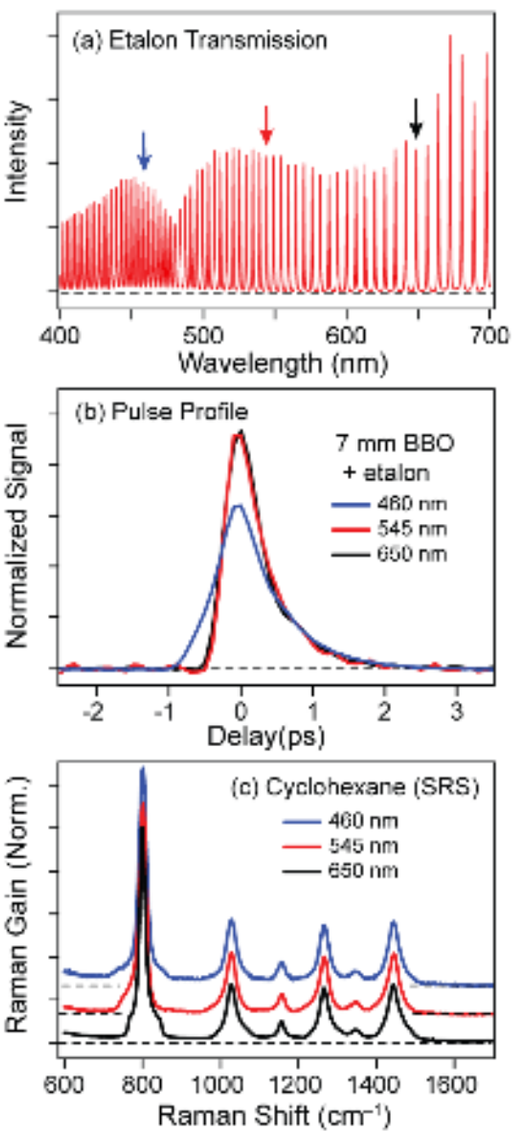

Figure 1. Transmission spectrum of the etalon (a), temporal pulse profiles after passing the output of a 7 mm BBO crystal through the etalon at representative wavelengths (b), and the resulting SRS spectra for neat cyclohexane (c).

The pump pulses at all three wavelengths in Figure 1 were generated using a 7 mm BBO crystal for SHG prior to the etalon. In each case, the pulse profile has an asymmetric shape with an exponential decay that is characteristic of the etalon filter. However, the temporal profile for 460 nm pulses has a slower rising edge compared with the pulses at longer wavelengths. In general, the rising edge of a transmitted pulse matches the temporal profile of the incident field, whereas the exponential decay on the falling edge reflects the ringdown of the etalon cavity. More efficient spectral narrowing at shorter wavelengths results in a longer pulse duration following SHG, and therefore a slower rising edge for the 460 nm pulses. In contrast, the 7 mm crystal provides less spectral compression at longer wavelengths, due to reduced group velocity dispersion, giving the sharper rising edges at 545 and 650 nm. The SRS spectra that we measure for neat cyclohexane (panel c) are essentially the same for all three Raman excitation wavelengths because the spectral resolution is determined by the trailing edge in the temporal profile of the pump pulse.

Figure 2 highlights the importance of the SHG crystal length in determining the temporal pulse profile, as well as the wavelength dependence of this process. The top panel of the figure shows the pulse profiles immediately after SHG at 460 nm. Spectral compression is related to the walk-off between incident and second harmonic fields in the SHG crystal,[26] and therefore depends on the length of the BBO crystal. This pathlength dependence is evident from the different temporal profiles for 460 nm pulses generated using the 7 and 25 mm BBO crystals. The longer (25 mm) crystal produces an extended tail on the rising edge of the pulse profile, compared with a more abrupt onset for pulses generated using the shorter 7 mm BBO. The broader phase-matching bandwidth for a 2 mm

BBO crystal (not shown) produces a pulse width of only 250 fs and almost no tail on the rising edge, but also provides significantly less spectral narrowing and therefore limits how much light passes through the etalon.

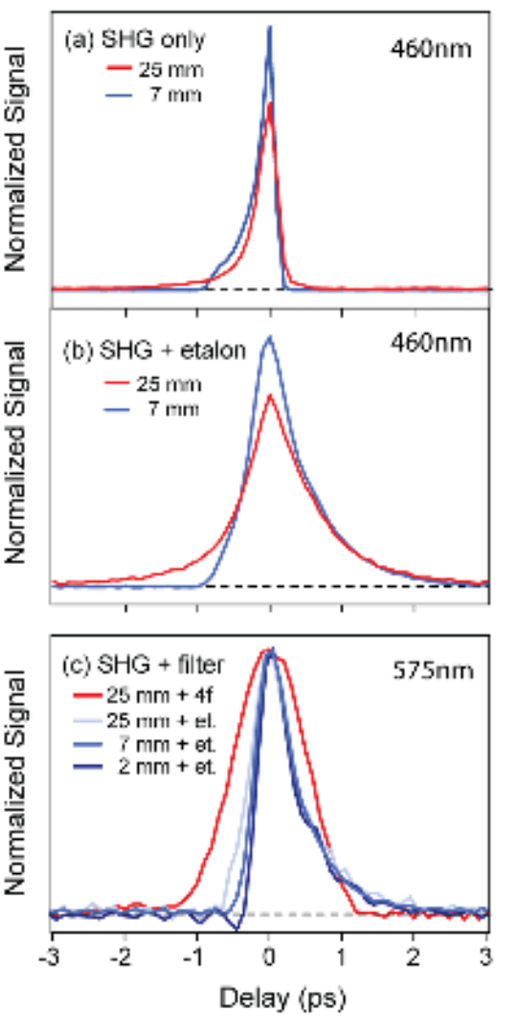

Figure 2. Temporal pulse profiles as a function of BBO crystal length and spectral filtering. The pulse profiles are normalized by area in (a) and (b), and by maximum amplitude in (c).

The temporal profiles obtained directly from the SHG crystal are not favorable for SRS, therefore we use the etalon filter to provide an asymmetric pulse shape that better matches the decay of the vibrational coherence in a stimulated Raman measurement. The

middle panel of Figure 2 shows the pulse profiles at 460 nm after passing through the etalon filter. Notably, the exponential tail on the trailing edge is essentially the same in both cases, because it reflects the transmission properties of the filter, even though the difference in the rising edge is preserved. Normalizing the pulse profiles by area emphasizes the difference in the relative intensity as a function of time for two pulses having the same total energy but different rise times. The 25 mm BBO gives a much slower rising edge, whereas the 7 mm BBO provides a better balance between spectral narrowing (for throughput) and a faster rising edge for reduced background signals.

Spectral compression is less efficient for SHG at longer wavelengths, but the pathlength of the crystal still affects the pulse profile. Figure 2c shows temporal profiles for pulses that were generated at 575 nm using three different BBO crystal lengths and then passed through the etalon. Although there is a smaller change in the rising edge as a function of crystal length compared with 460 nm, we show below that even a small difference can have a large impact on the background signal in resonance-enhanced SRS measurements. For comparison, Figure 2c also includes the temporal profile that we obtain using the 4*f* filter with 30 μm slit width. As shown previously, the 4*f* filter generates a symmetric pulse profile and gives substantially better SRS spectra compared with unfiltered pulses by eliminating broad bandwidth components that are generated at the front edge of the SHG crystal,[25] but this comes at the expense of background signals arising from resonant excitation.

The overall efficiency for generating tunable asymmetric Raman pump pulses with the etalon filter depends on several competing factors and varies with wavelength. In particular, the path length of the SHG crystal affects spectral compression, and therefore

impacts the transmission efficiency of the etalon (see Table 1). This effect is exacerbated by using the 4*f* filter to remove side-bands when the incident bandwidth is larger than the spacing between the transmission lines of the etalon. For example, removing the side-bands with a 150 μm slit width in the 4*f* filter results in an overall transmission efficiency of 28% for 575 nm pulses generated using the 25 mm BBO, 13% for the 7 mm BBO, and 6% for the 2 mm BBO (after compensating for reflection losses from the grating). For comparison, the combination of the etalon and 4*f* filter is only slightly less efficient than using a 30 μm slit width in the 4*f* filter (and no etalon) to provide similar spectral narrowing for any of the BBO crystals. In other words, the efficiency is primarily limited by the degree of spectral filtering in each case, but only the etalon gives the desired asymmetric temporal pulse profile.

Table 1: Transmission efficiencies at 575 nm for three different SHG crystal lengths[1]

	2 mm BBO	7 mm BBO	25 mm BBO	Relative Std. Dev.
Etalon transmission[2]	14.7 %	22.7 %	30.3 %	0.6%
Etalon + 4*f* Filter (150 μm slit)[3]	5.6 %	13.1 %	27.8 %	2.5%
4*f* Filter (30 μm slit)[4]	7.9 %	17.7 %	41.9 %	2.0%

[1] Measured with SHG input attenuated to give ~0.3 μJ/pulse at the sample position.
[2] Including side-bands.
[3] After removing etalon side-bands and accounting for grating efficiency.
[4] After accounting for grating efficiency.

The transmission efficiencies in Table 1 only account for losses due to the spectral filtering process. The overall efficiency for converting fundamental laser light to tunable picosecond pulses also depends on the optical parametric process (typically ~10-15% conversion into signal or idler), the SHG process (up to ~30% efficient depending on focal

conditions and crystal length), and transport to the sample (~30% efficiency, including two reflections from the grating in the 4*f* filter). All of these factors depend on wavelength and experimental conditions, and we typically attenuate the output of the OPA prior to SHG in order to obtain an optimum pulse energy of 0.5-1.0 μJ at the sample for SRS measurements.

Generating pump pulses at wavelengths below ~570 nm requires an additional stage of nonlinear conversion from idler to near IR prior to SHG with the long BBO crystal, which further limits the overall efficiency at these wavelengths. However, even at 460 nm we obtain at least ~0.25 μJ/pulse at the sample, which is sufficient for SRS measurements and is compensated by stronger Raman scattering at shorter wavelengths.[44,45] The overall conversion efficiency at 460 nm is ~0.02% compared with the 1.3 mJ of fundamental used to pump the OPA, and increases by about an order of magnitude at longer wavelengths. Considering that the combination of an OPA with SC-SHG and an etalon filter provides tunable pulses, this compares favorably with the efficiency of 0.3% that was reported previously for direct spectral filtering of the laser fundamental at 800 nm using an etalon with finesse of ~100.[33] The tunability of the direct filtering method is limited to angle tuning of the etalon across the bandwidth of the incident pulse, roughly 400 cm^{-1} for 35 fs pulses,[33] compared with the full range of visible wavelengths that we span using the output from a tunable fs OPA with SHG for partial spectral compression and an etalon to provide the desired pulse shape. This full tunability is only possible because of the increased transmission through the filter following partial spectral compression using SHG with a long BBO crystal.

B. Stimulated Raman Scattering

One of the most important benefits of the asymmetric pulse shape is the reduction of background signals originating from electronically resonant excitation. Figure 3 illustrates this point by comparing resonance-enhanced SRS spectra using symmetric and asymmetric pump pulses at 545 nm for Rh6G dissolved in methanol. Figure 3a shows the temporal profiles that we obtain by integrating over the 1033 cm^{-1} Raman band of neat methanol for pump pulses generated using either the 25 mm BBO and the 4*f* filter or the 7 mm BBO with the etalon filter. The temporal profiles are normalized to the area under the curve, which illustrates the higher peak intensity of the etalon pump pulse for the same total energy. Figure 3b shows the transient absorption (TA) signal for Rh6G under the same excitation conditions and integrated over the full ~40 nm range of probe wavelengths. The rising edge of the TA signal represents a convolution of the temporal profile of the pump pulse with the underlying dynamics of the molecule before the arrival of the probe pulse. The TA measurement highlights the different magnitudes of the background signal as a function of time delay for the two pulse shapes. The TA signal reaches the same total amplitude after ~2 ps because the total pulse energy is the same in each case, but the symmetric pulses excite a significantly larger fraction of Rh6G at negative delay times.

We typically record SRS spectra by setting the broadband probe pulse at the maximum of the ps pump pulse (a delay of t = 0 ps in the figure) in order to maximize the Raman signal. At this delay time, the signal includes contributions from both SRS and TA (see Figure 3c), but the latter is ~50% smaller for asymmetric pump pulses. Importantly, the TA signal contains overlapping contributions from GSB, ESA, and SE, all of which are time-

dependent and therefore complicate the interpretation of the background signal in SRS measurements due to the convolution of the fs dynamics of the molecule and the ps pulse shape. Moreover, the relative amplitude of the TA signal depends on the pump wavelength (see Figure S5), and becomes even larger for more resonant excitation wavelengths.

Comparing the signals in Figure 3 reveals that the background at t = 0 ps is smaller by nearly a factor of two for asymmetric pulses, without diminishing the strength of the Raman bands. In fact, after baseline correction the Raman bands are actually *stronger* in the case of the etalon filter, as shown in Figure 3d, where the Raman signal is ~1.5 times larger for asymmetric pump pulses. Alternatively, we can set the probe pulse to arrive 0.4 ps *before* the maximum of the symmetric pulse in order to achieve the same background signal as the asymmetric pulse (Figure 3e). Although the earlier time delay provides improved performance for the symmetric pulse,[25, 46, 47] the resulting Raman signal is still weaker than we observe using an asymmetric pulse with the same total energy (Figure 3f). The enhanced SRS signal for asymmetric pump pulses is a result of the higher peak intensity compared with symmetric pump pulses having the same total energy. The higher intensity of the asymmetric pulses at t = 0 initiates a stronger Raman response in combination with the broadband probe pulse. Having fewer pump photons arrive prior to the probe pulse also reduces the depletion of ground-state population before initiating the Raman measurement. Importantly, these observations suggest that the background signal can be reduced even further by attenuating the asymmetric pump pulses to give the same total Raman signal strength as the symmetric pulses.

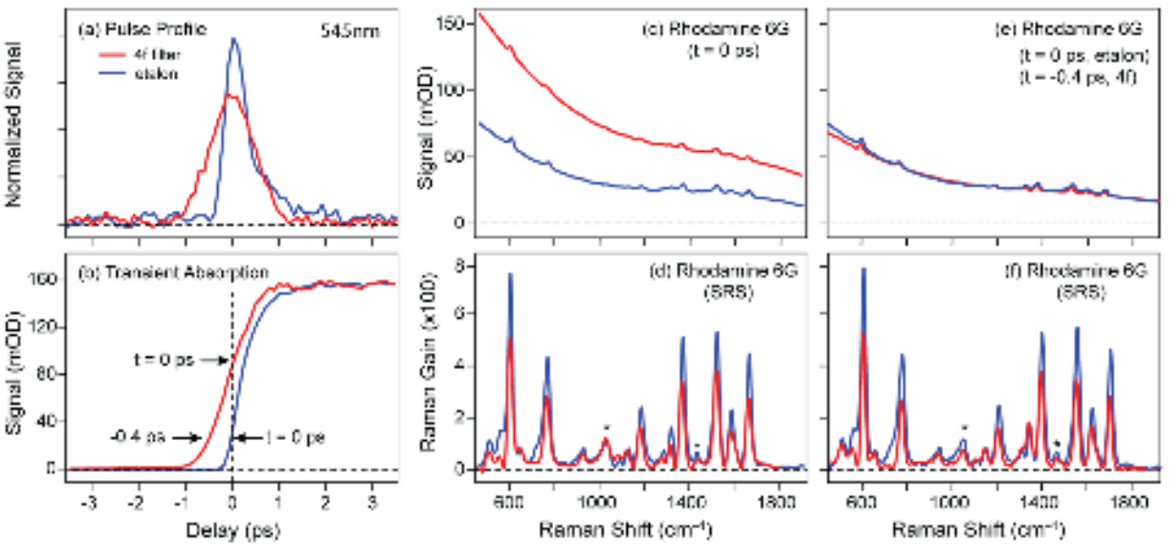

Figure 3. Comparison of symmetric and asymmetric pump pulses at 545 nm for resonance-enhanced SRS of rhodamine 6G in methanol. Temporal pulse profiles (a), time-dependent transient absorption signal (b), raw signal at specific time delays (c and e), and SRS spectra after baseline correction (d and f). The asterisks indicate solvent bands.

Considering the significant reduction of background signals using the etalon filter, it is useful to examine the dependence of the rising edge more closely. To this end, we illustrate the transition from asymmetric to symmetric pulse profile by varying the slit width in the 4*f* filter (Figure 4). All of the above measurements with the etalon used the 4*f* filter with a slit width of 150 μm in order to eliminate satellite peaks from adjacent transmission lines in the etalon filter without otherwise narrowing the bandwidth (see Figure S2). Here, however, we examine the effect of incrementally closing the slit to further alter the pulse profile. Figure 4 shows the variation in temporal and spectral profiles, as well as the resulting SRS spectra, for 555 nm pump pulses generated using the 7 mm BBO crystal and a combination of etalon and 4*f* filters. In order to facilitate the comparison of background signals, we attenuate the pump beam to give the same total pulse energy at the sample in each case. In the limit of a 30 μm slit width, the temporal profile is fully symmetric and matches the temporal and

spectral profiles that we achieve with the same slit width in the absence of the etalon filter. Intermediate slit widths of 60 and 100 μm only have a small impact on the spectral and temporal profiles compared with the 150 μm slit. However, even a small decrease of the bandwidth in the frequency domain, and therefore a small change in the rising edge of the temporal profile, has a significant impact on the relative intensity of the background signal in the SRS measurement (Figure 4c) and decreases the Raman signal strength (Figure 4d).

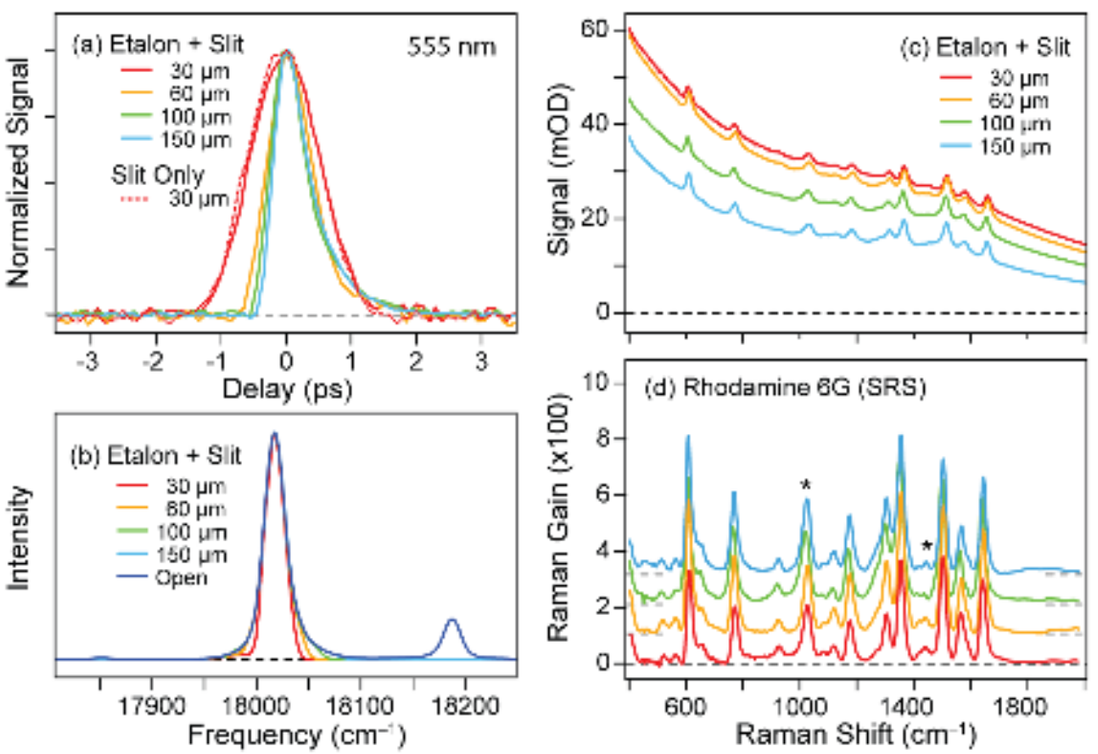

Figure 4. Temporal (a) and spectral (b) pulse profiles and the resulting spectra before (c) and after (d) baseline correction as a function of slit width in the 4*f* spatial filter. The SRS spectra in (d) are offset for clarity; asterisks indicate solvent bands.

Finally, we emphasize the finer tunability of the etalon filter by measuring resonance Raman excitation profiles across the first absorption band of Rh6G. Figure 5a shows the optical absorption spectrum of the dye in relation to the transmission of the etalon filter,

which we use to generate asymmetric pump pulses at six different wavelengths ranging from 600 to 540 nm. The resulting temporal pulse profiles from the etalon are essentially identical at all wavelengths over this 60 nm range (Figure S6). The raw SRS spectra (scaled to account for small differences in pump power at each wavelength) are shown in the middle panel of Figure 5. We reduce some of the spectra at shorter wavelengths by the amounts indicated in the figure in order to show all of the measurements on the same scale. Although the raw spectra for Rh6G still have relatively large background signals when using the etalon to produce electronically resonant pump pulses, the background is less than half the intensity that would be expected for pulses generated with the *4f* filter. Moreover, the asymmetric pulse profile reduces ground-state depletion and therefore gives stronger Raman signals.

After baseline correction we obtain the set of wavelength-dependent Raman spectra in Figure 5c. The vibrational frequencies and relative intensities are in excellent agreement with previously reported resonance Raman spectra for Rh6G in solution.[48-51] The Raman scattering signal for Rh6G increases substantially with excitation energy due to resonance enhancement. This resonance enhancement can also be visualized in a Raman gain profile, which tracks the intensity of each vibrational mode as a function of pump wavelength (Figure S7). The suppression of background signals and the high quality of the wavelength-dependent spectra for Rh6G highlight the benefits of using a low-finesse etalon filter to generate optimally shaped tunable picosecond pump pulses for resonance-enhanced SRS measurements.

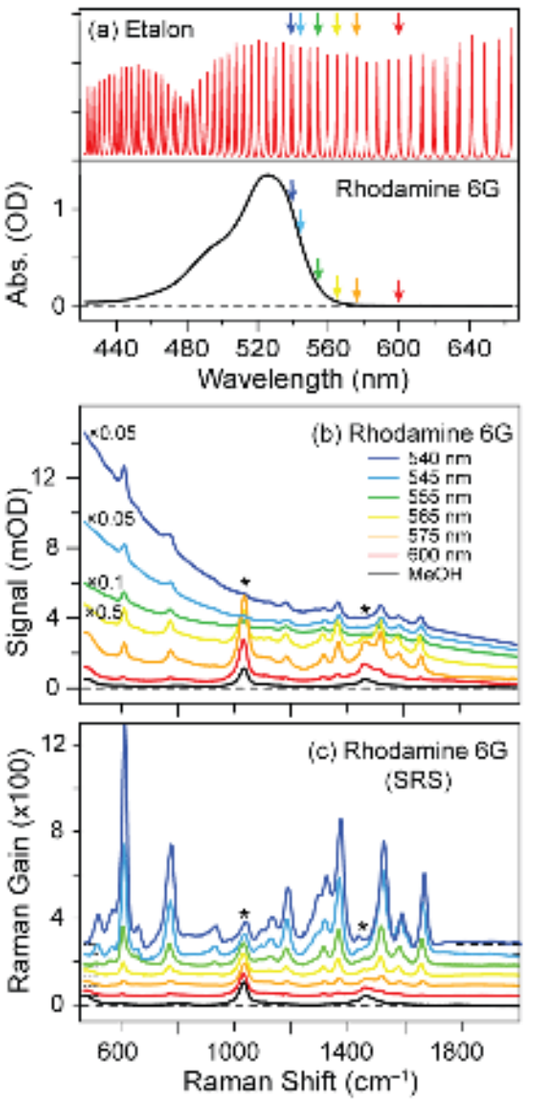

Figure 5. Raman excitation profiles for Rh6G in methanol. Etalon transmission and Rh6G absorption spectra (a), raw signal at t = 0 ps (b), and baseline-corrected SRS spectra (c). The arrows in (a) represent the Raman excitation wavelengths, asterisks in (b) and (c) indicate solvent bands, which do not increase on resonance, and the SRS spectra in (c) are offset for clarity.

IV. Conclusions

This contribution demonstrates for the first time the benefits of using a low-finesse etalon filter in combination with SC-SHG to generate tunable narrowband (picosecond) laser

pulses for resonance-enhanced FSRS measurements across the visible region of the spectrum. We showed that the etalon filter provides Raman excitation pulses with optimized pulse profiles across a ~200 nm wavelength range (460-650 nm). Importantly, the length of the SHG crystal preceding the etalon filter has a significant impact on the rising edge of the pump pulse profile, an effect that becomes more pronounced at shorter wavelengths. A judicious choice of crystal length allows optimization of the temporal pulse profile while still maintaining sufficiently narrow bandwidth for efficient transmission through the etalon filter. A 7 mm BBO crystal works well at the wavelengths we examined here, and the resulting asymmetric pulse shape allows significant baseline reduction for resonance-enhanced SRS measurements compared with symmetric pulse profiles obtained using a traditional 4*f* filter.

The superior performance of the asymmetric pulses generated using the low-finesse etalon filter is readily apparent from the suppression of electronically resonant background signal when the excitation pump is tuned into resonance with the first absorption band of Rh6G. In general, the etalon filter provides more intense Raman scattering signals while also minimizing background signals and reducing ground-state depletion of the target molecules, all of which simplify the processing and analysis of ground- and excited-state Raman spectra. The benefits of a tunable etalon filter open up the possibility of studying a wider variety of target molecules by taking better advantage of resonance-enhancement effects, especially when pursuing excited-state FSRS measurements with inherently weak signals and time-dependent backgrounds.

Supplementary Material

See the supplementary material for additional temporal and spectral intensity profiles, a description of the baselining method, and Raman excitation profiles for Rhodamine 6G.

Acknowledgements

This work was supported by the National Science Foundation (NSF) through grant number CHE-1956387. BK is grateful for summer research support from the Department of Chemistry at the University of Kansas while participating in Research Experiences for Undergraduates (REU) programming as a visiting student from Maryville University of Saint Louis.

Author Declarations

Conflict of interest

The authors have no conflicts to disclose.

Author Contributions

Data Availability

The data that support the findings of this study are available from the corresponding author upon reasonable request.

References

[1] Batignani, G.; Ferrante, C.; Scopigno, T. "Accessing Excited State Molecular Vibrations by Femtosecond Stimulated Raman Spectroscopy," *J. Phys. Chem. Lett.*, **11**(18), 7805-7813, (2020).

[2] Batignani, G.; Mai, E.; Fumero, G.; Mukamel, S.; Scopigno, T. "Absolute excited state molecular geometries revealed by resonance Raman signals," *Nat. Commun.*, **13**(1), 7770, (2022).

[3] Bera, K.; Douglas, C. J.; Frontiera, R. R. "Femtosecond stimulated Raman spectroscopy – guided library mining leads to efficient singlet fission in rubrene derivatives," *Chem. Sci.*, **12**(41), 13825-13835, (2021).

[4] Brown, K. E.; Singh, A. P. N.; Wu, Y.-L.; Mishra, A. K.; Zhou, J.; Lewis, F. D.; Young, R. M.; Wasielewski, M. R. "Tracking Hole Transport in DNA Hairpins Using a Phenylethynylguanine Nucleobase," *J. Am. Chem. Soc.*, **139**(34), 12084-12092, (2017).

[5] Burns, K. H.; Quincy, T. J.; Elles, C. G. "Excited-state resonance Raman spectroscopy probes the sequential two-photon excitation mechanism of a photochromic molecular switch," *J. Chem. Phys.*, **157**(23), (2022).

[6] Fang, C.; Frontiera, R. R.; Tran, R.; Mathies, R. A. "Mapping GFP structure evolution during proton transfer with femtosecond Raman spectroscopy," *Nature*, **462**(7270), 200-204, (2009).

[7] Fang, C.; Tang, L.; Oscar, B. G.; Chen, C. "Capturing Structural Snapshots during Photochemical Reactions with Ultrafast Raman Spectroscopy: From Materials Transformation to Biosensor Responses," *J. Phys. Chem. Lett.*, **9**(12), 3253-3263, (2018).

[8] Fang, C.; Tang, L. "Mapping Structural Dynamics of Proteins with Femtosecond Stimulated Raman Spectroscopy," *Annu. Rev. Phys. Chem.*, **71**, 239-265, (2020).

[9] Ferrante, C.; Batignani, G.; Pontecorvo, E.; Montemiglio, L. C.; Vos, M. H.; Scopigno, T. "Ultrafast Dynamics and Vibrational Relaxation in Six-Coordinate Heme Proteins Revealed by Femtosecond Stimulated Raman Spectroscopy," *J. Am. Chem. Soc.*, **142**(5), 2285-2292, (2020).

[10] Ferrante, C.; Pontecorvo, E.; Cerullo, G.; Vos, M. H.; Scopigno, T. "Direct observation of subpicosecond vibrational dynamics in photoexcited myoglobin," *Nat. Chem.*, **8**(12), 1137-1143, (2016).

[11] Frontiera, R. R.; Fang, C.; Dasgupta, J.; Mathies, R. A. "Probing structural evolution along multidimensional reaction coordinates with femtosecond stimulated Raman spectroscopy," *PCCP*, **14**(2), 405-414, (2012).

[12] Fumero, G.; Batignani, G.; Dorfman, K. E.; Mukamel, S.; Scopigno, T. "On the Resolution Limit of Femtosecond Stimulated Raman Spectroscopy: Modelling Fifth-Order Signals with Overlapping Pulses," *ChemPhysChem*, **16**(16), 3438-3443, (2015).

[13] McCamant, D. W.; Kukura, P.; Yoon, S.; Mathies, R. A. "Femtosecond broadband stimulated Raman spectroscopy: Apparatus and methods," *Rev. Sci. Instrum.*, **75**(11), 4971-4980, (2004).

[14] Frontiera, R. R.; Mathies, R. A. "Femtosecond stimulated Raman spectroscopy," *Laser Photonics Rev.*, **5**(1), 102-113, (2011).

[15] Kukura, P.; McCamant, D. W.; Mathies, R. A. "Femtosecond Stimulated Raman Spectroscopy," *Annu. Rev. Phys. Chem.*, **58**, 461-488, (2007).

[16] Burns, K. H.; Srivastava, P.; Elles, C. G. "Absolute Cross Sections of Liquids from Broadband Stimulated Raman Scattering with Femtosecond and Picosecond Pulses," *Anal. Chem.*, **92**(15), 10686-10692, (2020).

[17] Mukamel, S.; Biggs, J. D. "Communication: Comment on the effective temporal and spectral resolution of impulsive stimulated Raman signals," *J. Chem. Phys.*, **134**(16), (2011).

[18] Dietze, D. R.; Mathies, R. A. "Femtosecond Stimulated Raman Spectroscopy," *ChemPhysChem*, **17**(9), 1224-1251, (2016).

[19] Pontecorvo, E.; Ferrante, C.; Elles, C. G.; Scopigno, T. "Structural Rearrangement Accompanying the Ultrafast Electrocyclization Reaction of a Photochromic Molecular Switch," *The Journal of Physical Chemistry B*, **118**(24), 6915-6921, (2014).

[20] Burns, K. H.; Elles, C. G. "Ultrafast Dynamics of a Molecular Switch from Resonance Raman Spectroscopy: Comparing Visible and UV Excitation," *J. Phys. Chem. A*, **126**(35), 5932-5939, (2022).

[21] Quincy, T. J.; Barclay, M. S.; Caricato, M.; Elles, C. G. "Probing Dynamics in Higher-Lying Electronic States with Resonance-Enhanced Femtosecond Stimulated Raman Spectroscopy," *J. Phys. Chem. A*, **122**(42), 8308-8319, (2018).

[22] Zhu, L.; Liu, W.; Fang, C. "A versatile femtosecond stimulated Raman spectroscopy setup with tunable pulses in the visible to near infrared," *Applied Physics Letters*, **105**(4), (2014).

[23] Liu, X.; Li, B.-H.; Liang, Y.; Zeng, W.; Li, H.; Zhou, C.; Ren, Z.; Yang, X. "Efficient generation of narrowband picosecond pulses from a femtosecond laser," *Rev. Sci. Instrum.*, **92**(8), (2021).

[24] Kang, D.-g.; Woo, K. C.; Kang, D. H.; Park, C.; Kim, S. K. "Improved spectral resolution of the femtosecond stimulated Raman spectroscopy achieved by the use of the 2nd-order diffraction method," *Scientific Reports*, **11**(1), 3361, (2021).

[25] Pontecorvo, E.; Ferrante, C.; Elles, C. G.; Scopigno, T. "Spectrally tailored narrowband pulses for femtosecond stimulated Raman spectroscopy in the range 330-750 nm," *Opt. Express*, **21**(6), 6866-6872, (2013).

[26] Pontecorvo, E.; Kapetanaki, S. M.; Badioli, M.; Brida, D.; Marangoni, M.; Cerullo, G.; Scopigno, T. "Femtosecond stimulated Raman spectrometer in the 320-520nm range," *Opt. Express*, **19**(2), 1107-1112, (2011).

[27] Redeckas, K.; Voiciuk, V.; Vengris, M. "A tunable femtosecond stimulated Raman scattering system based on spectrally narrowed second harmonic generation," *Lithuanian Journal of Physics*, **56**(1), (2016).

[28] Grumstrup, E. M.; Chen, Z.; Vary, R. P.; Moran, A. M.; Schanze, K. S.; Papanikolas, J. M. "Frequency Modulated Femtosecond Stimulated Raman Spectroscopy of Ultrafast Energy Transfer in a Donor–Acceptor Copolymer," *The Journal of Physical Chemistry B*, **117**(27), 8245-8255, (2013).

[29] Batignani, G.; Pontecorvo, E.; Giovannetti, G.; Ferrante, C.; Fumero, G.; Scopigno, T. "Electronic resonances in broadband stimulated Raman spectroscopy," *Scientific Reports*, **6**(1), 18445, (2016).

[30] Batignani, G.; Ferrante, C.; Fumero, G.; Martinati, M.; Scopigno, T. "Femtosecond stimulated Raman spectroscopy," *Nat. Rev. Methods Primers*, **4**(1), 34, (2024).

[31] Artes Vivancos, J. M.; van Stokkum, I. H. M.; Saccon, F.; Hontani, Y.; Kloz, M.; Ruban, A.; van Grondelle, R.; Kennis, J. T. M. "Unraveling the Excited-State Dynamics and Light-Harvesting Functions of Xanthophylls in Light-Harvesting Complex II Using Femtosecond Stimulated Raman Spectroscopy," *J. Am. Chem. Soc.*, **142**(41), 17346-17355, (2020).

[32] Bera, K.; Kwang, S. Y.; Cassabaum, A. A.; Rich, C. C.; Frontiera, R. R. "Facile Background Discrimination in Femtosecond Stimulated Raman Spectroscopy Using a Dual-Frequency Raman Pump Technique," *J. Phys. Chem. A*, **123**(37), 7932-7939, (2019).

[33] Hoffman, D. P.; Valley, D.; Ellis, S. R.; Creelman, M.; Mathies, R. A. "Optimally shaped narrowband picosecond pulses for femtosecond stimulated Raman spectroscopy," *Opt. Express*, **21**(18), 21685-21692, (2013).

[34] Lynch, P. G.; Das, A.; Alam, S.; Rich, C. C.; Frontiera, R. R. "Mastering Femtosecond Stimulated Raman Spectroscopy: A Practical Guide," *ACS Phys. Chem. Au*, **4**(1), 1-18, (2024).

[35] Hecht, E. *Optics*, 5th ed.; Pearson Education Limited, 2017.

[36] Rich, C. C.; Frontiera, R. R. "Vibronic Coupling and Exciton Chirality: Electronic and Structural Rearrangement between Helical to Zero Momentum Molecular Exciton States," *J. Phys. Chem. C*, **125**(39), 21511-21520, (2021).

[37] Clapham, M. L.; Das, A.; Douglas, C. J.; Frontiera, R. R. "Killer Phonon Caught: Femtosecond Stimulated Raman Spectroscopy Identifies Phonon-Induced Control of Photophysics in Rubrene Derivatives," *J. Am. Chem. Soc.*, **146**(29), 19939-19950, (2024).

[38] Hoffman, D. P.; Ellis, S. R.; Mathies, R. A. "Characterization of a Conical Intersection in a Charge-Transfer Dimer with Two-Dimensional Time-Resolved Stimulated Raman Spectroscopy," *J. Phys. Chem. A*, **118**(27), 4955-4965, (2014).

[39] Ellis, S. R.; Hoffman, D. P.; Park, M.; Mathies, R. A. "Difference Bands in Time-Resolved Femtosecond Stimulated Raman Spectra of Photoexcited Intermolecular Electron Transfer from Chloronaphthalene to Tetracyanoethylene," *J. Phys. Chem. A*, **122**(14), 3594-3605, (2018).

[40] Valley, D. T.; Hoffman, D. P.; Mathies, R. A. "Reactive and unreactive pathways in a photochemical ring opening reaction from 2D femtosecond stimulated Raman," *PCCP*, **17**(14), 9231-9240, (2015).

[41] Li, H.; Luo, W.; Li, G.; Zhang, G.; Zhang, P.; Li, C.; Gu, Y. "A practical wide-field Raman imaging method with high spectral and spatial resolution," *Rev. Sci. Instrum.*, **89**(8), (2018).

[42] Amiel, Y.; Nedvedski, R.; Mandelbaum, Y.; Tischler, Y. R.; Tischler, H. "Super-Spectral-Resolution Raman spectroscopy using angle-tuning of a Fabry-Pérot etalon with application to diamond characterization," *Spectrochimica Acta Part A: Molecular and Biomolecular Spectroscopy*, **325**, 125038, (2025).

[43] Silva, W. R.; Keller, E. L.; Frontiera, R. R. "Determination of Resonance Raman Cross-Sections for Use in Biological SERS Sensing with Femtosecond Stimulated Raman Spectroscopy," *Anal. Chem.*, **86**(15), 7782-7787, (2014).

[44] Dudik, J. M.; Johnson, C. R.; Asher, S. A. "Wavelength dependence of the preresonance Raman cross sections of CH3CN, SO42−, ClO4−, and NO3−," *J. Chem. Phys.*, **82**(4), 1732-1740, (1985).

[45] Schomacker, K. T.; Delaney, J. K.; Champion, P. M. "Measurements of the absolute Raman cross sections of benzene," *J. Chem. Phys.*, **85**(8), 4240-4247, (1986).

[46] Ferrante, C.; Batignani, G.; Fumero, G.; Pontecorvo, E.; Virga, A.; Montemiglio, L. C.; Cerullo, G.; Vos, M. H.; Scopigno, T. "Resonant broadband stimulated Raman scattering in myoglobin," *Journal of Raman Spectroscopy*, **49**(6), 913-920, (2018).

[47] Yoon, S.; McCamant, D. W.; Kukura, P.; Mathies, R. A.; Zhang, D.; Lee, S.-Y. "Dependence of line shapes in femtosecond broadband stimulated Raman spectroscopy on pump-probe time delay," *J. Chem. Phys.*, **122**(2), (2004).

[48] Shim, S.; Stuart, C. M.; Mathies, R. A. "Resonance Raman Cross-Sections and Vibronic Analysis of Rhodamine 6G from Broadband Stimulated Raman Spectroscopy," *ChemPhysChem*, **9**(5), 697-699, (2008).

[49] Guthmuller, J.; Champagne, B. "Resonance Raman Scattering of Rhodamine 6G as Calculated by Time-Dependent Density Functional Theory: Vibronic and Solvent Effects," *J. Phys. Chem. A*, **112**(14), 3215-3223, (2008).

[50] Jensen, L.; Schatz, G. C. "Resonance Raman Scattering of Rhodamine 6G as Calculated Using Time-Dependent Density Functional Theory," *J. Phys. Chem. A*, **110**(18), 5973-5977, (2006).

[51] Chen, C.; Zhu, L.-d.; Fang, C. "Femtosecond stimulated Raman line shapes: Dependence on resonance conditions of pump and probe pulses†," *Chinese Journal of Chemical Physics*, **31**(4), 492-502, (2018).